

Numerical solution of the Fokker–Planck equation with variable coefficients[☆]

Arnold D. Kim^{*}, Paul Tranquilli

School of Natural Sciences, P.O. Box 2039, University of California, Merced, Merced, CA 95344, USA

Received 13 July 2007; received in revised form 31 August 2007; accepted 23 September 2007

Abstract

We study the numerical solution of the Fokker–Planck equation. This equation gives a good approximation to the radiative transport equation when scattering is peaked sharply in the forward direction which is the case for light propagation in tissues, for example. We derive first the numerical solution for the problem with constant coefficients. This numerical solution is constructed as an expansion in plane wave solutions. Then we extend that result to take into account coefficients that vary spatially. This extension leads to a coupled system of initial and final value problems. We solve this system iteratively. Numerical results show the utility of this method.

© 2007 Elsevier Ltd. All rights reserved.

Keywords: Radiative transport equation; Fokker–Planck approximation; Variable coefficients

1. Introduction

Light propagation in random media such as biological tissues is governed by the theory of radiative transport [1]. The radiative transport equation takes into account absorption and scattering due to inhomogeneities. It is an integral–partial differential equation. Analytical solutions are available only for relatively simple problems [2]. Hence, we must use numerical methods to compute solutions.

Computing numerical solutions to solve the radiative transport is inherently challenging. First of all one must take into account the several independent variables for the direction and position. In fact, computational methods may face difficulty in resolving all of these variables adequately without exceeding available resources. In addition, one must take into account accurately the coupling between these spatial and directional variables in the radiative transport equation. This coupling can be difficult to treat numerically because the dependent variable, the specific intensity, can be discontinuous with respect to direction.

[☆]This work is supported by the National Science Foundation (DMS-0504858) and the US Department of Energy through the UC Merced Center for Computational Biology.

^{*}Corresponding author. Tel.: +1 209 228 2951; fax: +1 209 228 4053.

E-mail addresses: adkim@ucmerced.edu (A.D. Kim), ptranquilli@ucmerced.edu (P. Tranquilli).

For several applications of radiative transport theory such as light propagation in tissues [3], cosmic rays in the atmosphere [4] and electron beams for cancer therapy [5] among others, scattering is peaked sharply in the forward scattering direction. For this situation, solving the radiative transport equation numerically becomes even more difficult. The sharp forward scattering peak requires high resolution with respect to the direction variables to approximate the integral operator in the transport equation accurately. An alternative to solving the radiative transport equation for sharply peaked forward scattering is to replace it with the Fokker–Planck equation. It is just for forward-peaked scattering that the Fokker–Planck equation provides a good approximation [3]. The Fokker–Planck approximation takes forward-peaked scattering into account analytically by replacing the integral operator in the transport equation by a simpler differential operator. Hence, the Fokker–Planck equation is easier to solve than the radiative transport equation.

The Fokker–Planck equation as an approximation to the radiative transport equation has been studied extensively. In particular, the asymptotic limits in which the Fokker–Planck equation is valid have been established [6,7]. Moreover, numerical solutions of the Fokker–Planck equation have been shown to compare well with those of the radiative transport equation [3]. Hence, we do not pursue validating the Fokker–Planck equation as an approximation to the radiative transport equation in this work.

The Fokker–Planck equation is one example of a two-way diffusion equation [8–10] or a backward–forward parabolic equation [11,12]. Computing numerical solutions of backward–forward parabolic equations requires non-standard numerical methods to take into account the coupling between backward and forward diffusions without over-regularizing the problem. There have been several studies of numerical methods for backward–forward diffusion equations. Vanaja and Kellogg [13] give a finite difference method that requires a delicate iterative scheme to handle the finite difference scheme where singularities can form. Vanaja [14] has applied this method to the Fokker–Planck equation with no absorption and a constant scattering coefficient. Han and Yin [15] have developed a non-overlapping domain decomposition method for solving the finite difference approximation. Aziz and Liu [16,17] have transformed the backward–forward diffusion equation into a first-order system of symmetric-positive differential equations in the sense of Friedrichs which they solve using finite elements. In contrast, Lu [18] and French [19,20] have developed Galerkin methods without transforming the problem. Ref. [21] provides an overview of these finite element methods. Lu and Maubach [22] have extended the finite element method due to Lu [18] to a generalized problem that includes variable coefficients.

The aforementioned methods use sophisticated techniques to compute numerical solutions. Here, we seek to solve the Fokker–Planck equation in a simpler way for use in solving practical problems such as light propagation in tissues. Kim and Keller [3] have solved the Fokker–Planck equation with constant coefficients in a simple way using so-called plane wave solutions. These plane wave solutions are calculated numerically through the solution of an associated eigenvalue problem. The eigenvectors form a basis that provides a natural way to represent the numerical solution. This numerical method is analogous to the discrete-ordinate method using the eigenmode expansion technique for the radiative transport equation [1]. Kim and Moscoso [23] have extended the plane wave solution method to higher dimensional problems. Here, we analyze this method further and extend it to allow for variable coefficients.

Our motivation in studying the variable coefficients problem is its importance in applications of light propagation in tissues containing an obstacle. This obstacle scattering problem is a model for tissues containing a tumor or another physiological anomaly. Understanding the obstacle scattering problem in tissues is a key step in developing methods for diagnosing tissue health. However, results for this problem are limited due to a lack of computational methods to solve this problem. These results may find use in other applications also.

The remainder of this paper is as follows. We first review the theory of radiative transport and the Fokker–Planck approximation for sharply peaked forward scattering in Section 2. In Section 3, we review the numerical method due to Kim and Keller [3] to solve the Fokker–Planck equation with constant coefficients. In Section 4, we extend that method to allow for spatially varying coefficients. This method yields a coupled system of initial and final value problems. We solve this system using an iterative method that uses the trapezoidal method to integrate the differential equations. In Section 5, we show numerical results that demonstrate the utility of this method. Section 6 is the conclusions.

2. Radiative transport theory and the Fokker–Planck approximation

Light propagation in random media is governed by the radiative transport equation:

$$\mathbf{\Omega} \cdot \nabla I + \mu_a I - \mu_s L I = 0. \tag{1}$$

Here, I is the specific intensity. It gives the power flowing in direction $\mathbf{\Omega}$ at position r . We denote the absorption and scattering coefficients by μ_a and μ_s , respectively. The scattering operator L is defined as

$$L I = -I + \int_{S^2} p(\mathbf{\Omega} \cdot \mathbf{\Omega}') I(\mathbf{\Omega}', r) d\mathbf{\Omega}'. \tag{2}$$

The scattering phase function p gives the fraction of light incident in direction $\mathbf{\Omega}'$ that scatters in direction $\mathbf{\Omega}$. Integration in (2) is taken over the unit sphere S^2 . The anisotropy factor g is defined in terms of p as

$$g = 2\pi \int_{-1}^1 p(\mu) \mu d\mu. \tag{3}$$

For tissues, $g \sim 1$ because scattering is peaked sharply in the forward scattering direction corresponding to $\mu = \mathbf{\Omega} \cdot \mathbf{\Omega}' \sim 1$.

When scattering is peaked sharply in the forward scattering direction, the Fokker–Planck approximation:

$$L I \approx \frac{1}{2} \mu_{tr} \Delta_{\Omega} I, \tag{4}$$

with $\mu_{tr} = \mu_s(1 - g)$ and Δ_{Ω} denoting the spherical laplacian, is a good approximation. We call (1) with (4) the Fokker–Planck equation. One obtains the Fokker–Planck approximation (4) through asymptotic analysis of (2) for sharply peaked forward scattering [3]. The Fokker–Planck equation is easier to solve numerically because this approximation is done analytically. Hence, (4) does not require the high angular resolution that (2) does when scattering is sharply peaked.

To solve the radiative transport or Fokker–Planck equation in a domain D with boundary ∂D , we must prescribe boundary conditions. Proper boundary conditions give the light at the boundary directed into the medium. Hence, we prescribe boundary conditions of the form

$$I(\mathbf{\Omega}, r_b) = I_b(\mathbf{\Omega}, r_b), \quad r_b \in \partial D, \quad \mathbf{\Omega} \cdot \hat{n}(r_b) < 0, \tag{5}$$

with $\hat{n}(r_b)$ denoting the unit outward normal at r_b . Here, I_b denotes the specific intensity at the boundary directed into the domain.

3. Problem formulation

We study light propagation in a slab $0 < z < d$ composed of an absorbing and scattering medium in which scattering is peaked sharply in the forward scattering direction. A plane wave is incident on the boundary plane $z = 0$ in direction $\mathbf{\Omega}_0$. That is the only source of light in this problem. We parameterize the unit direction vector $\mathbf{\Omega}$ by the cosine of the polar angle $\mu = \cos \theta$ and the azimuthal angle φ .

For this problem, the specific intensity I satisfies the Fokker–Planck equation:

$$\mu \frac{\partial I}{\partial z} + \mu_a I = \frac{1}{2} \mu_{tr} \left\{ \frac{\partial}{\partial \mu} \left[(1 - \mu^2) \frac{\partial I}{\partial \mu} \right] + \frac{1}{1 - \mu^2} \frac{\partial^2 I}{\partial \varphi^2} \right\}, \quad -1 \leq \mu \leq 1, \quad -\pi \leq \varphi \leq \pi, \quad 0 < z < d, \tag{6}$$

subject to the boundary conditions

$$I(\mu, \varphi, 0) = F_0 \delta(\mu - \mu_0) \delta(\varphi - \varphi_0), \quad 0 < \mu \leq 1, \quad -\pi \leq \varphi \leq \pi, \tag{7}$$

and

$$I(\mu, \varphi, d) = 0, \quad -1 \leq \mu < 0, \quad -\pi \leq \varphi \leq \pi. \tag{8}$$

We represent I as a Fourier series in φ

$$I(\mu, \varphi, z) = \sum_{n=-\infty}^{\infty} \Psi_n(\mu, z) e^{in\varphi}, \tag{9}$$

with

$$\Psi_n(\mu, z) = \frac{1}{2\pi} \int_{-\pi}^{\pi} I(\mu, \varphi, z) e^{-in\varphi} d\varphi. \tag{10}$$

Each Fourier mode Ψ_n satisfies

$$\mu \frac{\partial \Psi_n}{\partial z} + \mu_a \Psi_n = \frac{1}{2} \mu_{tr} \left\{ \frac{\partial}{\partial \mu} \left[(1 - \mu^2) \frac{\partial \Psi_n}{\partial \mu} \right] - \frac{n^2}{1 - \mu^2} \Psi_n \right\}, \quad -1 \leq \mu \leq 1, \quad 0 < z < d, \tag{11}$$

subject to the boundary conditions

$$\Psi_n(\mu, 0) = \frac{F_0}{2\pi} \delta(\mu - \mu_0) e^{-in\varphi_0}, \quad 0 < \mu \leq 1, \tag{12}$$

and

$$\Psi_n(\mu, d) = 0, \quad -1 \leq \mu < 0. \tag{13}$$

In (11)–(13), we see that each Fourier mode Ψ_n is decoupled from all others. Therefore, developing a method to solve (11)–(13) for n fixed can be applied for each value of n needed. Hence, we study the problem with $n = 0$ only. In fact, we generalize the problem slightly for the discussion that appears below. In particular, we seek the numerical solution of the boundary value problem:

$$\mu \frac{\partial \Psi}{\partial z} + \mu_a \Psi = \frac{1}{2} \mu_{tr} \frac{\partial}{\partial \mu} \left[(1 - \mu^2) \frac{\partial \Psi}{\partial \mu} \right], \quad -1 \leq \mu \leq 1, \quad 0 < z < d, \tag{14a}$$

$$\Psi(\mu, 0) = f(\mu), \quad 0 < \mu \leq 1, \tag{14b}$$

$$\Psi(\mu, d) = g(\mu), \quad -1 \leq \mu < 0. \tag{14c}$$

Here, μ_a and μ_{tr} are functions of z and the function f and g are general functions defined over the half ranges $0 < \mu \leq 1$ and $-1 \leq \mu < 0$, respectively.

Boundary value problem (14) is a parabolic differential equation in which μ is the space-like variable since $\partial^2 \Psi / \partial \mu^2$ occurs in it. The time-like variable is z where $\mu > 0$ and $-z$ where $\mu < 0$. Such an equation is called a two-way diffusion [8–10] or a backward–forward parabolic equation [11,12]. The boundary value problem (14) is a well-posed problem [8]. Fig. 1 shows a sketch of the domain for this problem.

4. Numerical solution for the constant coefficients problem

We solve (14) first for the case in which $\mu_a = \alpha$ and $\mu_{tr} = 2\sigma$, where α and σ are positive constants. For that case, we seek a numerical solution based on the analytical separation of variable solution.

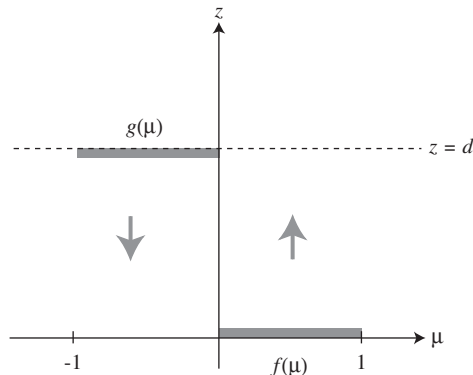


Fig. 1. A sketch of the domain of the boundary value problem (14) we study here. Eq. (14a) is a parabolic differential equation in which μ is the space-like variable. The time-like variable is z where $\mu > 0$ and $-z$ where $\mu < 0$. Boundary condition (14b) prescribes Ψ at $z = 0$ over the half-range $0 < \mu \leq 1$. Boundary condition (14c) Ψ at $z = d$ over the half-range $-1 \leq \mu < 0$.

4.1. Separation of variable solution

We seek the general solution of

$$\mu \frac{\partial \Psi}{\partial z} + \alpha \Psi - \sigma \frac{\partial}{\partial \mu} \left[(1 - \mu^2) \frac{\partial \Psi}{\partial \mu} \right] = 0 \tag{15}$$

of the form $\Psi(\mu, z) = e^{\lambda z} v(\mu)$. Substitution of this general solution form into (15) yields the eigenvalue problem

$$\lambda \mu v + \alpha v - \sigma \frac{\partial}{\partial \mu} \left[(1 - \mu^2) \frac{\partial v}{\partial \mu} \right] = 0. \tag{16}$$

This eigenvalue problem has several useful properties [24] that we list below:

1. Eq. (16) has both positive eigenvalues called $\lambda_n > 0$ with $n > 0$ and negative eigenvalues called $\lambda_n < 0$ with $n < 0$.
2. For $\alpha \neq 0$, there is no zero eigenvalue.
3. For any pair $[\lambda_n, v_n(\mu)]$ satisfying (16), the pair $[-\lambda_n, v_n(-\mu)]$ satisfies it also. Hence, we assume that the eigenvalues are ordered and indexed so that

$$\lambda_{-n} = -\lambda_n, \quad v_{-n}(\mu) = v_n(-\mu), \quad n = 1, 2, \dots \tag{17}$$

4. Two pairs $[\lambda_m, v_m(\mu)]$ and $[\lambda_n, v_n(\mu)]$ each satisfying (16) satisfy also the orthogonality relation:

$$(\lambda_m - \lambda_n) \int_{-1}^1 v_m(\mu) v_n(\mu) \mu \, d\mu = 0. \tag{18}$$

In light of (18) and because

$$\int_{-1}^1 v_{-n}(\mu) v_{-n}(\mu) \mu \, d\mu = - \int_{-1}^1 v_n(\mu) v_n(\mu) \mu \, d\mu, \tag{19}$$

due to (17), we normalize the eigenfunctions according to

$$\int_{-1}^1 v_n^2(\mu) \mu \, d\mu = -\text{sgn}(n). \tag{20}$$

The general solution of (15) in the slab $0 < z < d$ is given by the superposition of eigenfunctions:

$$\Psi(\mu, z) = \sum_{n=1}^{\infty} [c_{-n} e^{-\lambda_n z} v_n(-\mu) + c_n e^{\lambda_n(z-d)} v_n(\mu)]. \tag{21}$$

We have used (17) in writing this general solution. Substituting (21) into the boundary condition (14b), we obtain

$$\sum_{n=1}^{\infty} [c_{-n} v_n(-\mu) + c_n e^{-\lambda_n d} v_n(\mu)] = f(\mu), \quad 0 < \mu \leq 1. \tag{22}$$

Substituting (21) into the boundary condition (14c), we obtain

$$\sum_{n=1}^{\infty} c_{-n} e^{-\lambda_n d} v_n(-\mu) + c_n v_n(\mu) = g(\mu), \quad -1 \leq \mu < 0. \tag{23}$$

In principle, (22) and (23) define a linear system for the expansion coefficients c_{-n} and c_n . However, the eigenfunctions do not satisfy an orthogonality relation on the half-ranges: $-1 \leq \mu < 0$ and $0 < \mu \leq 1$. Hence, we cannot determine explicit expressions for c_{-n} and c_n without solving the problem first. It is at this point in the analysis where we introduce numerical calculations.

4.2. Numerical solution

To compute a numerical solution, we solve the eigenvalue problem (16) numerically. To do so, we introduce the $2N$ -point Gauss–Legendre quadrature rule:

$$\int_{-1}^1 f(\mu) d\mu \approx \sum_{j=1}^{2N} f(\mu_j) w_j, \quad (24)$$

with μ_j denoting the quadrature abscissas and w_j denoting the quadrature weights for $j = 1, \dots, 2N$. Because the number of abscissas and weights are even, $\mu_{2N-j+1} = -\mu_j$ and $w_{2N-j+1} = w_j$ for $j = 1, \dots, 2N$. We introduce the approximant $v_j \approx v(\mu_j)$ which satisfies

$$\lambda \mu_j v_j + \alpha v_j - \sigma [\beta_{j+1/2}(v_{j+1} - v_j) - \beta_{j-1/2}(v_j - v_{j-1})] = 0, \quad j = 1, \dots, 2N, \quad (25)$$

with

$$\beta_{j+1/2} = \frac{\gamma_{j+1/2}}{w_j} \frac{1}{\mu_{j+1} - \mu_j}, \quad \beta_{j-1/2} = \frac{\gamma_{j-1/2}}{w_j} \frac{1}{\mu_j - \mu_{j-1}}. \quad (26)$$

Here, $\gamma_{1/2} = 0$ and

$$\gamma_{j+1/2} = \gamma_{j-1/2} + 2\mu_j w_j, \quad j = 1, \dots, 2N. \quad (27)$$

By construction, $\gamma_{2N+1/2} = 0$. Hence, numerical boundary conditions are not needed. This finite difference scheme is due to Morel [25].

We denote by \mathbf{v} the $2N$ -vector whose entries are $\mathbf{v} = (v_1, \dots, v_{2N})$. Rewriting (25) in terms of \mathbf{v} , we obtain

$$\lambda M \mathbf{v} + \alpha \mathbf{v} - \sigma L \mathbf{v} = 0. \quad (28)$$

with $M = \text{diag}(\mu_1, \dots, \mu_{2N})$ and L denoting the tridiagonal matrix corresponding to the finite difference formula in (25) whose non-zero entries are given by

$$L_{jj} = -\beta_{j+1/2} - \beta_{j-1/2}, \quad j = 1, \dots, N, \quad (29a)$$

$$L_{j,j-1} = \beta_{j-1/2}, \quad j = 2, \dots, N, \quad (29b)$$

$$L_{j,j+1} = \beta_{j+1/2} \quad j = 1, \dots, N-1. \quad (29c)$$

The eigenvalue problem (28) has $2N$ pairs of eigenvalues λ_n and corresponding eigenvectors \mathbf{v}_n . Due to the symmetries inherent in the Gauss–Legendre quadrature rule and the eigenvalue problem (28), we can show that for each positive eigenvalue $\lambda_n > 0$ with eigenvector \mathbf{v}_n , there is another eigenvalue $-\lambda_n$ with eigenvector $\tilde{\mathbf{v}}_n$, where the components V_{jn} of \mathbf{v}_n and \tilde{V}_{jn} of $\tilde{\mathbf{v}}_n$ are related by

$$V_{jn} = \tilde{V}_{2N-j+1,n}. \quad (30)$$

Just as the eigenfunctions $v_n(\mu)$ are normalized according to (20), the eigenvectors \mathbf{v}_n are normalized according to

$$\sum_{j=1}^{2N} V_{jn}^2 \mu_j w_j = -1, \quad n = 1, \dots, N. \quad (31)$$

We now introduce the approximant $\Psi_j(z) \approx \Psi(\mu_j, z)$ which we represent as the superposition of the eigenvectors:

$$\Psi_j(z) = \sum_{n=1}^N [\tilde{a}_n e^{-\lambda_n z} V_{2N-j+1,n} + \bar{b}_n e^{\lambda_n(z-d)} V_{jn}], \quad j = 1, \dots, 2N. \quad (32)$$

We determine the expansion coefficients by imposing the boundary conditions (14b) and (14c) for each $\mu_j > 0$ and $\mu_j < 0$, respectively, resulting in

$$\sum_{n=1}^N [\bar{a}_n V_{2N-j+1,n} + \bar{b}_n e^{-\lambda_n d} V_{jn}] = f(\mu_j), \quad j = N + 1, \dots, 2N, \tag{33a}$$

$$\sum_{n=1}^N [\bar{a}_n e^{-\lambda_n d} V_{2N-j+1,n} + \bar{b}_n V_{jn}] = g(\mu_j), \quad j = 1, \dots, N. \tag{33b}$$

Eq. (33) defines a $2N \times 2N$ linear system for the $2N$ coefficients a_n and b_n . Upon solution of this system, we obtain $\Psi_j(z)$ through evaluation of (32).

We give the procedure to solve numerically the boundary value problem (14) with constant coefficients below:

1. Specify α and σ .
2. Choose N and compute the $2N$ -point Gauss–Legendre quadrature rule.
3. Evaluate $M = \text{diag}(\mu_1, \dots, \mu_{2N})$ and L defined in (29).
4. Solve (28) for the N positive eigenvalues λ_n and corresponding eigenvectors \mathbf{v}_n .
5. Normalize the eigenvectors \mathbf{v}_n according to (31).
6. Solve (33) for \bar{a}_n and \bar{b}_n .
7. Calculate the approximant $\Psi_j(z)$ for each value of z desired by evaluating (32).

The numerical solution discussed above is analogous to the discrete ordinate method for the radiative transport equation. The convergence of the discrete ordinate method is well established [26–29]. The methods used for establishing convergence for the discrete ordinate method apply to this problem in an analogous way. Hence, we do not discuss it here.

5. Numerical solution for the variable coefficients problem

We now consider the case in which μ_a and μ_{tr} are functions of z . We seek a numerical solution by variation of parameters based on the solution for the constant coefficients problem. From this analysis, we derive a coupled system of initial and final value problems. We propose an iterative scheme to solve this system.

5.1. Variation of parameters

We seek the solution of the variable coefficients problem:

$$\mu \frac{\partial \Psi}{\partial z} + \mu_a(z) \Psi = \frac{1}{2} \mu_{tr}(z) \frac{\partial}{\partial \mu} \left[(1 - \mu^2) \frac{\partial \Psi}{\partial \mu} \right]. \tag{34}$$

We introduce the approximant $\Psi_j(z) \approx \Psi(\mu_j, z)$ with μ_j denoting the Gauss–Legendre quadrature points as in the previous section. The vector $\Psi(z)$ whose entries are given by $\Psi = (\Psi_1(z), \dots, \Psi_{2N}(z))$ satisfies

$$M \frac{\partial \Psi}{\partial z} + \mu_a(z) \Psi = \frac{1}{2} \mu_{tr}(z) L \Psi, \tag{35}$$

with M and L defined the same as for (28). In light of the numerical solution for the constant coefficients problem given by (32), we seek the solution of (36) of the form

$$\Psi_j(z) = \sum_{n=1}^N [a_n(z) V_{2N-j+1,n} + b_n(z) V_{jn}], \quad j = 1, \dots, 2N. \tag{36}$$

The eigenvalues λ_n and eigenvectors \mathbf{v}_n in (36) correspond to the solution of (28) with constant coefficients $\mu_a = \alpha$ and $\mu_{tr} = 2\sigma$. Substituting (36) into (35) and using (28), we obtain

$$\sum_{n=1}^N \left\{ \left[\mu_j \frac{da_n}{dz} + \left(1 + \frac{\tilde{\sigma}}{\sigma} \right) \lambda_n \mu_j a_n + \left(\tilde{\alpha} - \frac{\alpha}{\sigma} \tilde{\sigma} \right) a_n \right] V_{2N-j+1,n} + \left[\mu_j \frac{db_n}{dx} - \left(1 + \frac{\tilde{\sigma}}{\sigma} \right) \lambda_n \mu_j b_n + \left(\tilde{\alpha} - \frac{\alpha}{\sigma} \tilde{\sigma} \right) b_n \right] V_{jn} \right\} = 0, \quad j = 1, \dots, 2N. \tag{37}$$

In (37), we have introduced the notation

$$\tilde{\alpha}(z) = \mu_a(z) - \alpha, \quad \tilde{\sigma}(z) = \frac{1}{2}\mu_{tr}(z) - \sigma. \tag{38}$$

The eigenvectors satisfy the orthogonality relations

$$\sum_{j=1}^{2N} V_{jm} V_{jn} \mu_j w_j = -\delta_{mn}, \quad \sum_{j=1}^{2N} V_{2N-j+1,m} V_{2N+j-1,n} \mu_j w_j = \delta_{mn}, \tag{39}$$

with δ_{mn} denoting the Kronecker delta. Hence, multiplying (37) by $V_{2N-j+1,m} w_j$ and summing over $j = 1, \dots, 2N$, we obtain

$$\frac{da_m}{dz} + \left(1 + \frac{\tilde{\sigma}}{\sigma} \right) \lambda_m a_m + \left(\tilde{\alpha} - \frac{\alpha}{\sigma} \tilde{\sigma} \right) \sum_{n=1}^N [P_{mn} a_n + Q_{mn} b_n] = 0, \quad m = 1, \dots, N, \tag{40}$$

with

$$P_{mn} = \sum_{j=1}^{2N} V_{2N-j+1,m} V_{2N-j+1,n} w_j = \sum_{j=1}^{2N} V_{jm} V_{jn} w_j, \tag{41}$$

and

$$Q_{mn} = \sum_{j=1}^{2N} V_{2N-j+1,m} V_{jn} w_j = \sum_{j=1}^{2N} V_{jm} V_{2N-j+1,n} w_j. \tag{42}$$

The sums in (41) and (42) are equal due to the symmetry of the eigenvectors given in (30). Similarly, by multiplying (37) by $V_{jm} w_j$ and summing over $j = 1, \dots, 2N$, we obtain

$$-\frac{db_m}{dz} + \left(1 + \frac{\tilde{\sigma}}{\sigma} \right) \lambda_m b_m + \left(\tilde{\alpha} - \frac{\alpha}{\sigma} \tilde{\sigma} \right) \sum_{n=1}^N [Q_{mn} a_n + P_{mn} b_n] = 0, \quad m = 1, \dots, N. \tag{43}$$

Eqs. (40) and (43) define $2N$ coupled first-order differential equations for the $2N$ coefficients $a_n(z)$ and $b_n(z)$. The time-like variable in (40) is z , so we need to prescribe an initial condition at $z = 0$. The time-like variable in (43) is $-z$, so we need to prescribe a final condition at $z = d$. Evaluating (37) at $z = 0$ and imposing (14b) at each of the quadrature abscissas $\mu_j > 0$, we obtain after rearranging terms

$$\sum_{n=1}^N a_n(0) V_{2N-j+1,n} = f(\mu_j) - \sum_{n=1}^N b_n(0) V_{jn}, \quad j = N + 1, \dots, 2N. \tag{44}$$

Similarly, evaluating (37) at $z = d$ and imposing (14c) at each of the quadrature abscissas $\mu_j < 0$, we obtain after rearranging terms

$$\sum_{n=1}^N b_n(d) V_{jn} = g(\mu_j) - \sum_{n=1}^N a_n(d) V_{2N-j+1,n}, \quad j = 1, \dots, N. \tag{45}$$

5.2. Numerical solution of the coupled initial and final value problems

We introduce notation to write the coupled initial and final value problems above more compactly. Let $\mathbf{a}(z)$ and $\mathbf{b}(z)$ be the N -vectors whose components are $\mathbf{a}(z) = (a_1(z), \dots, a_{2N}(z))$ and $\mathbf{b}(z) = (b_1(z), \dots, b_{2N}(z))$,

respectively. Let \mathbf{f} and \mathbf{g} be the N -vectors whose entries are given by $\mathbf{f} = (f(\mu_{N+1}), \dots, f(\mu_{2N}))$ and $\mathbf{g} = (g(\mu_1), \dots, g(\mu_N))$, respectively. Let P and Q be the $N \times N$ matrices whose entries are given by P_{mn} given in (42) and Q_{mn} given in (43). Furthermore, let $A = \text{diag}(\lambda_1, \dots, \lambda_N)$ and $A, B, C,$ and D be the $N \times N$ matrices whose entries are given by

$$A_{jn} = V_{2N-j+1,n}, \quad j = 1, \dots, N, \quad n = 1, \dots, N, \tag{46a}$$

$$B_{jn} = V_{2N-j+1,n}, \quad j = N + 1, \dots, 2N, \quad n = 1, \dots, N, \tag{46b}$$

$$C_{jn} = V_{jn}, \quad j = 1, \dots, N, \quad n = 1, \dots, N, \tag{46c}$$

$$D_{jn} = V_{jn}, \quad j = N + 1, \dots, 2N, \quad n = 1, \dots, N. \tag{46d}$$

Using these quantities in (40)–(45), we obtain the initial value problem for $\mathbf{a}(z)$:

$$\frac{d\mathbf{a}}{dz} + \left(1 + \frac{\tilde{\sigma}}{\sigma}\right)A\mathbf{a} + \left(\tilde{\alpha} - \frac{\alpha}{\sigma}\tilde{\sigma}\right)[P\mathbf{a} + Q\mathbf{b}] = 0, \quad 0 < z < d, \tag{47a}$$

$$B\mathbf{a}(0) = \mathbf{f} - D\mathbf{b}(0), \tag{47b}$$

and the final value problem for $\mathbf{b}(z)$:

$$-\frac{d\mathbf{b}}{dz} + \left(1 + \frac{\tilde{\sigma}}{\sigma}\right)A\mathbf{b} + \left(\tilde{\alpha} - \frac{\alpha}{\sigma}\tilde{\sigma}\right)[Q\mathbf{a} + P\mathbf{b}] = 0, \quad 0 < z < d, \tag{48a}$$

$$C\mathbf{b}(d) = \mathbf{g} - A\mathbf{a}(d). \tag{48b}$$

To solve (47) and (48), we propose an iterative method. Suppose we have chosen a suitable integration method to solve a system of first-order differential equations. We discuss a specific choice for an integration method below. We give the procedure for the iterative method below:

1. Initialize $\mathbf{a}^{(0)}(z) = 0$ and $\mathbf{b}^{(0)}(z) = 0$.
2. Assign $n:=1$
3. Compute $\mathbf{a}^{(n)}(0)$ by solving (47b).
4. Integrate numerically (47a) from $z = 0$ to d .
5. Compute $\mathbf{b}^{(n)}(d)$ by solving (48b).
6. Integrate numerically (48a) from $z = d$ to 0 .
7. Assign $n:=n + 1$.
8. Repeat Steps 3–7 until

$$\max(\|\mathbf{a}^{(n)} - \mathbf{a}^{(n-1)}\|, \|\mathbf{b}^{(n)} - \mathbf{b}^{(n-1)}\|) < \varepsilon,$$

with ε denoting a user-defined termination parameter.

For each iteration described above, we must integrate numerically a first-order system of the form

$$\frac{d\mathbf{a}}{dz} + r(z)A\mathbf{a} + s(z)P\mathbf{a} = -s(z)Q\mathbf{b}, \tag{49}$$

from $z = 0$ to d . The coefficients r and s are defined as

$$r(z) = 1 + \frac{1}{\sigma}\tilde{\sigma}(z), \tag{50a}$$

$$s(z) = \tilde{\alpha}(z) - \frac{\alpha}{\sigma}\tilde{\sigma}(z). \tag{50b}$$

In (49) \mathbf{b} is assumed to be known since it is from a previous iteration. From the solution of (28), we know empirically that the diagonal matrix A has the properties that $\min(\lambda_n) \ll 1$ and $\max(\lambda_n) \gg 1$. For example, with $N = 16$, $\alpha = 0.1$ and $\sigma = 0.05$, we find that $\min(\lambda_n) = 0.2227$ and $\max(\lambda_n) = 223.7908$. Hence, (49) is stiff. We

choose to integrate (49) with the trapezoid rule. It is fully implicit, second-order accurate and unconditionally stable.

Consider a grid with equi-spaced points defined at $z_k = kh$ for $k = 0, \dots, N_z$ with $h = d/N_z$. We introduce the notation $r_k = r(z_k)$, $s_k = s(z_k)$ and the approximant $\mathbf{a}_k \approx \mathbf{a}(z_k)$ which satisfies

$$\frac{\mathbf{a}_k - \mathbf{a}_{k-1}}{h} + \frac{1}{2}[r_k \Lambda \mathbf{a}_k + r_{k-1} \Lambda \mathbf{a}_{k-1} + s_k P \mathbf{a}_k + s_{k-1} P \mathbf{a}_{k-1}] = -\frac{1}{2}[s_k Q \mathbf{b}_k + s_{k-1} Q \mathbf{b}_{k-1}], \quad k = 1, \dots, N_x. \quad (51)$$

Rearranging terms in (51), we arrive at the linear system:

$$\left[I + \frac{h}{2}(r_k \Lambda + s_k P) \right] \mathbf{a}_k = \left[I - \frac{h}{2}(r_k \Lambda + s_k P) \right] \mathbf{a}_{k-1} - \frac{h}{2}[s_k Q \mathbf{b}_k + s_{k-1} Q \mathbf{b}_{k-1}], \quad k = 1, \dots, N_x, \quad (52)$$

with I denoting the $N \times N$ identity matrix. Similarly, to integrate the equation

$$-\frac{d\mathbf{b}}{dz} + r(z)\Lambda \mathbf{b} + s(z)P \mathbf{b} = -s(z)Q \mathbf{a}, \quad (53)$$

from $z = d$ to 0 with \mathbf{a} assumed to be known, we introduce the approximant $\mathbf{b}_k \approx \mathbf{b}(z_k)$ and solve the linear system

$$\left[I + \frac{h}{2}(r_k \Lambda + s_k P) \right] \mathbf{b}_k = \left[I - \frac{h}{2}(r_{k+1} \Lambda + s_{k+1} P) \right] \mathbf{b}_{k+1} - \frac{h}{2}[s_k Q \mathbf{a}_k + s_{k+1} Q \mathbf{a}_{k+1}], \quad k = N_x - 1, \dots, 0. \quad (54)$$

Once \mathbf{a} and \mathbf{b} have been computed using the iterative finite difference method described above, we compute the solution through evaluation of (37).

6. Numerical results

To evaluate the numerical method presented in Section 5, we solved numerically

$$\mu \frac{\partial \Psi}{\partial x} + \alpha \Psi = \sigma \frac{\partial}{\partial \mu} \left[(1 - \mu^2) \frac{\partial \Psi}{\partial \mu} \right], \quad -1 \leq \mu \leq 1, \quad 0 < z < 1, \quad (55a)$$

$$\Psi(\mu, 0) = 1, \quad 0 < \mu \leq 1, \quad (55b)$$

$$\Psi(\mu, 1) = 2, \quad -1 \leq \mu < 0, \quad (55c)$$

with $\alpha = 0.02$, $\sigma = 0.01$. A plot of the computed solution to this problem appears in Fig. 2. Fig. 2 shows clearly the singularities near $\mu = 0$ at $z = 0$ and 1.

We computed the solution of boundary value problem (55) numerically using two different methods. For the first method, we followed the procedure given in Section 4 with the constant coefficients $\alpha = 0.02$ and $\sigma = 0.01$. We denote that numerical solution by Ψ_1 . For the second method, we followed the procedure given in Section 5. For that solution, we used the eigenvectors corresponding to the constant coefficients problem with $\alpha = 0.01$ and $\sigma = 0.005$. Hence, we solved (47) and (48) with $\tilde{\alpha} = 0.01$ and $\tilde{\sigma} = 0.005$. We denote that numerical solution by Ψ_2 . For both sets of computations, we have set the number of quadrature points to be $2N = 32$.

In Table 1, we show the results from solving (55) using the procedure given in Fig. 3. For this case, we set $h = 0.0025$. We reached a tolerance of $\varepsilon = 1 \times 10^{-12}$ within 10 iterations. We varied both the slab thickness and the strength of the perturbations to the coefficients by large amounts and found that neither affected substantially the number of iterations required by this computation for this problem.

We compared the solutions Ψ_1 and Ψ_2 from the two different numerical methods. In Fig. 3, we show the solutions at the boundaries $z = 0$ and 1 as a function of μ . The circle symbols correspond to Ψ_1 and the solid curves correspond to Ψ_2 . We observe that both methods are able to resolve the singularities at $\mu = 0$ well. Moreover, the two computed solutions are indistinguishable from one another.

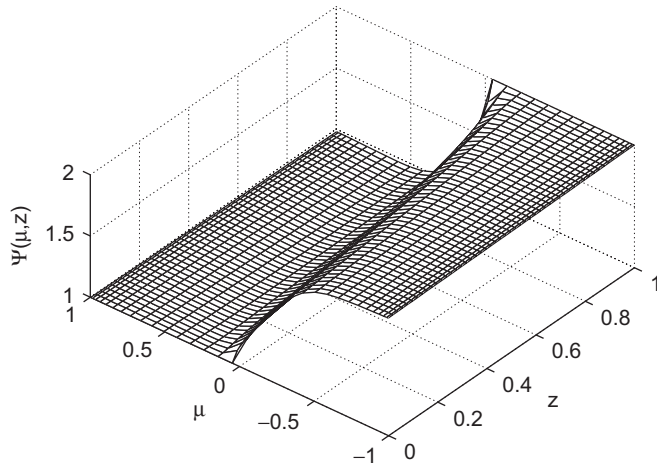


Fig. 2. The computed solution to the boundary value problem (55).

Table 1
Convergence of iterations for the boundary value problem (55) with $h = 0.0025$ and $N = 32$

Iteration (n)	$\ \mathbf{a}^{(n)} - \mathbf{a}^{(n-1)}\ _2$	$\ \mathbf{b}^{(n)} - \mathbf{b}^{(n-1)}\ _2$
1	3.338	0.56049
2	0.095068	0.016118
3	0.0027319	0.00046304
4	7.8479×10^{-5}	1.3301×10^{-5}
5	2.2544×10^{-6}	3.8208×10^{-7}
6	6.4758×10^{-8}	1.0976×10^{-8}
7	1.8602×10^{-9}	3.1533×10^{-10}
8	5.3462×10^{-11}	9.0456×10^{-12}
9	1.5170×10^{-12}	2.5645×10^{-13}
10	4.1888×10^{-14}	3.7118×10^{-15}

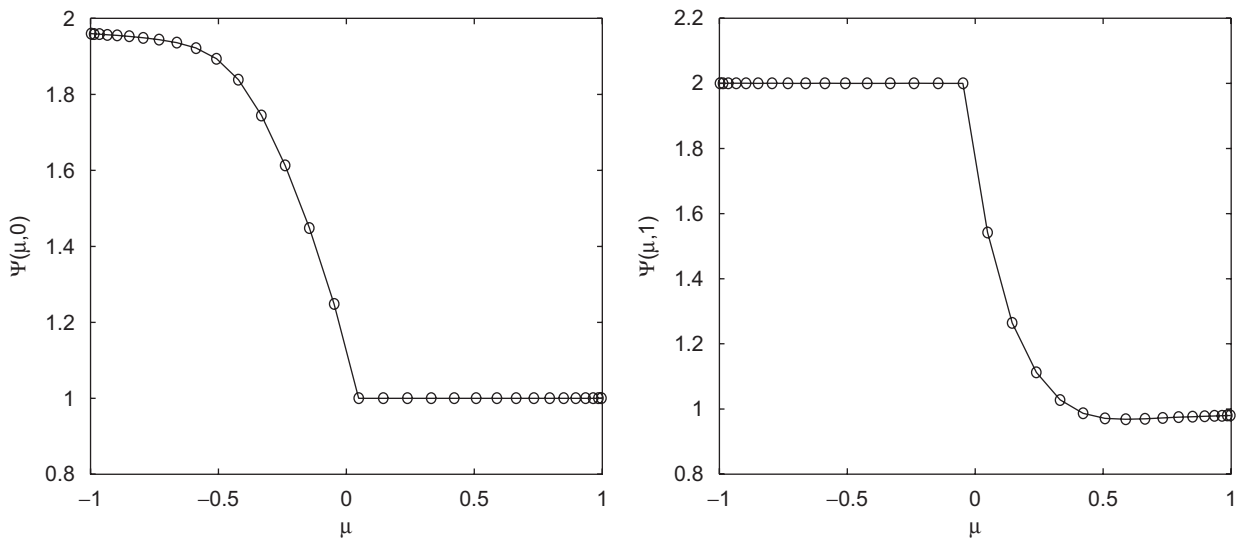


Fig. 3. Comparison of the solution of (55) computed using the iterative finite difference scheme (solid curves) and the separation of variable solution (circles) at $z = 0$ (left plot) and $z = 1$ (right plot).

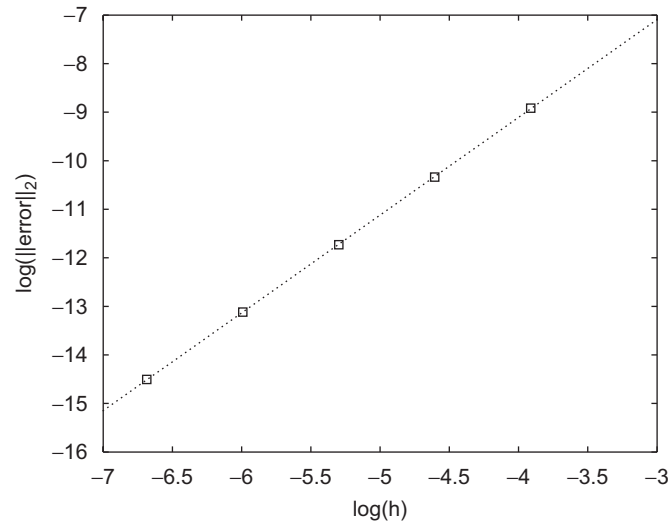


Fig. 4. The error defined by (56) which compares the solutions computed using the iterative finite difference method and the separation of variable solution. The linear fit shown as the dotted curve yields a slope 2.0142 indicating the second-order convergence of the finite difference scheme.

To validate the second-order convergence of the trapezoid rule that we used to solve the system of coupled initial–final value problems resulting in Ψ_2 , we computed an error through comparison with the solution Ψ_1 . This error is defined as

$$\text{error} = \frac{\|\Psi_1 - \Psi_2\|_2}{\|\Psi_1\|_2}. \quad (56)$$

We plot this error for various values of h on a log–log plot in Fig. 4. In addition, we computed a linear fit to the data (given by the dotted curve in Fig. 4) and determined that the slope is 2.0142 indicating clearly a second-order convergence.

Next, we applied the iterated finite difference method to solve a more challenging problem. In particular, we solved numerically (34) with

$$\mu_a(z) = 0.01 + 5e^{-500(z-0.6)^2}, \quad (57)$$

and

$$\mu_{tr}(z) = 0.01 + 5e^{-400(z-0.4)^2}, \quad (58)$$

subject to the boundary conditions

$$\Psi(\mu, 0) = e^{-100(\mu-1)^2}, \quad 0 < \mu \leq 1, \quad (59)$$

and

$$\Psi(\mu, 1) = 0, \quad -1 \leq \mu < 0. \quad (60)$$

This problem models a plane wave incident normally at $z = 0$ on a plane-parallel slab of tissue of unit thickness. No light enters into the other end of the slab at $z = 1$. The slab of tissue has an absorbing inhomogeneity given by the second term of (57) and a scattering inhomogeneity given by the second term of (58).

For this example, we have deviated away slightly from an actual physical problem. In particular, the boundary condition at $z = 0$ for a plane wave normally incident on the slab is proportional to $\delta(\mu - 1)$ as we described above in Section 3. In boundary condition (59), we have replaced this delta function by a narrow Gaussian to regularize the problem. Moreover, the magnitude of the absorbing and scattering inhomogeneities

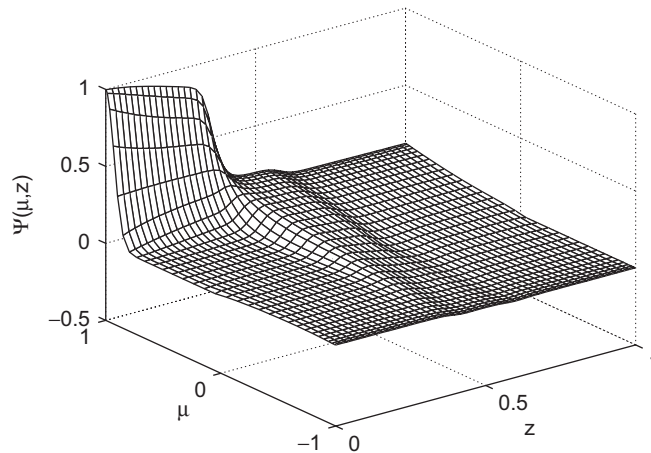


Fig. 5. The radiance as a function of z and μ with θ denoting the polar angle for the example problem (34) with (57)–(60) computed using the iterative finite difference method.

are much larger than what one encounters in tissue optics. However, we have chosen these parameter values to highlight the utility of the numerical method.

A plot of the computed solution to (34) with (57)–(60) appears in Fig. 5. This computed solution required 61 iterations to reach a tolerance of $\varepsilon = 1 \times 10^{-12}$ with $h = 0.0025$. Substantially more iterations were required for this problem compared with the previous one due to the additional complexity introduced by the variable coefficients. We found that the number of iterations required by this computation does not depend on the thickness of the slab. However, by reducing the strength of the inhomogeneities, we found that the number of iterations required by this computation reduced. Hence, we have determined that the number of iterations required depends on the magnitude of the perturbation away from the associated constant coefficient problem and not the size of the domain.

A heuristic explanation of this problem is as follows. Light is injected into the slab at $z = 0$ in a narrow cone of directions about $\mu = 1$. As that light propagates into the slab, the medium absorbs and scatters it with strengths $\alpha = 0.01$ and $\sigma = 0.005$, respectively. Scattering causes the radiance, that is peaked about $\mu = 1$, to be spread away from $\mu = 1$. Absorption causes an overall attenuation of the radiance. Near $z = 0.4$, the radiance interacts with the scattering inhomogeneity. The scattering inhomogeneity causes the radiance's peak about $\mu = 1$ to spread even more than the scattering due to the background medium. Near $z = 0.6$, the radiance interacts with absorbing inhomogeneity. The absorbing inhomogeneity causes the radiance to attenuate overall even more than the absorption due to the background medium.

The characteristics of the computed solution shown in Fig. 5 are consistent with this explanation. In Fig. 5, we see that the radiance's peak near $\mu = 1$ spreads and attenuates due to scattering and absorption, respectively. Near $z = 0.4$, we observe that the radiance spreads substantially away from $\mu = 1$. Near $z = 0.6$, we observe that the radiance undergoes substantial attenuation.

7. Conclusions

We have derived a numerical solution of a boundary value problem for the Fokker–Planck equation with variable coefficients. This variable coefficients problem is important for studying light propagation in tissues containing an obstacle such as a tumor. The Fokker–Planck equation is one example of a backward–forward heat or two-way diffusion equation. In particular, this problem models light propagation in tissues that scatter light strongly in the forward direction.

We have solved this problem numerically by extending the numerical solution for a related constant coefficients problem through variation of parameters. In doing so, we have derived a reduced system of initial and final value problems. Because the differential equations in this system are stiff, we have integrated them using a second-order, fully implicit trapezoid rule. We have solved this system by an iterative method. We have

found that the number of iterations required by this method does not depend on the size of the domain. Rather, the number of iterations depends on size of the inhomogeneities modeled by the variable coefficients.

We have compared the solution computed using this method with another method and verified its second-order accuracy. Finally, we have used this method to solve a problem related to light propagation in a slab of tissue with absorbing and scattering inhomogeneities. This method was able to compute a solution to this problem readily. These results suggest that this numerical method should be extremely useful for calculating light propagation in biological tissues with inhomogeneous absorption and scattering coefficients.

Acknowledgment

The authors wish to thank Miguel Moscoso for his helpful comments while preparing this work.

References

- [1] Ishimaru A. Wave propagation and scattering in random media. New York: IEEE Press; 1997.
- [2] Case KM, Zweifel PF. Linear transport theory. Reading, MA: Addison-Wesley; 1960.
- [3] Kim AD, Keller JB. Light propagation in biological tissue. *J Opt Soc Am A* 2003;20:92–8.
- [4] Eyges L. Multiple scattering with energy loss. *Phys Rev* 1948;74:1534–5.
- [5] Brahme A. Current algorithms for computed beam dose planning. *Radiother Oncol* 1985;3:347–62.
- [6] Pomraning GC. The Fokker–Planck operator as an asymptotic limit. *Math Models Methods Appl Sci* 1992;2:21–36.
- [7] Larsen EW. The linear Boltzmann equation in optically thick systems with forward-peaked scattering. *Prog Nucl Energy* 1999;107:413–23.
- [8] Fisch NJ, Kruskal MD. Separating variables in two-way diffusion equations. *J Math Phys* 1980;21:740–50.
- [9] Beals R. Partial-range completeness and existence of solutions to two-way diffusion equations. *J Math Phys* 1981;22:954–60.
- [10] Andersson F, Helander P, Anderson D, Smith H, Lisak M. Approximate solutions of two-way diffusion equations. *Phys Rev E* 2002;65:036502.
- [11] Keller JB, Weinberger HF. Boundary and initial-boundary value problems for separable backward–forward parabolic problems. *J Math Phys* 1997;38:4343–53.
- [12] Knessl C, Keller JB. Ray solution of a backward–forward parabolic problem for data-handling systems. *Eur J Appl Math* 2000;11:1–12.
- [13] Vanaja V, Kellogg RB. Iterative methods for a forward–backward heat equation. *SIAM J Numer Anal* 1990;27:622–35.
- [14] Vanaja V. Numerical solution of a simple Fokker–Planck equation. *Appl Numer Math* 1992;9:533–40.
- [15] Han H, Yin D. A non-overlap domain decomposition method for the forward–backward heat equation. *J Comput Appl Math* 2003;159:35–44.
- [16] Aziz AK, Liu J-L. A Galerkin method for the forward–backward heat equation. *Math Comput* 1991;56:35–44.
- [17] Aziz AK, Liu J-L. A weighted least squares method for the backward–forward heat equation. *SIAM J Numer Anal* 1991;28:156–67.
- [18] Lu H. Galerkin and weighted Galerkin methods for the forward–backward heat equation. *Numer Math* 1997;75:339–56.
- [19] French DA. Discontinuous Galerkin finite element methods for a forward–backward heat equation. *Appl Numer Math* 1998;28:37–44.
- [20] French DA. Continuous Galerkin finite element methods for a forward–backward heat equation. *Numer Methods Partial Differential Equations* 1999;15:257–65.
- [21] Aziz AK, French DA, Jensen S, Kellogg RB. Origins, analysis, numerical analysis, and numerical approximation of a forward–backward parabolic equation. *Math Model Numer Anal* 1999;33:895–922.
- [22] Lu H, Maubach J. A finite element method and variable transformations for a forward–backward heat equation. *Numer Math* 1998;81:249–72.
- [23] Kim AD, Moscoso M. Beam propagation in sharply peaked forward scattering media. *J Opt Soc Am A* 2004;21:797–803.
- [24] Kim AD. Transport theory for light propagation in biological tissue. *J Opt Soc Am A* 2004;21:820–7.
- [25] Morel JE. An improved Fokker–Planck angular differencing scheme. *Nucl Sci Eng* 1985;89:131–6.
- [26] Keller HB. Approximate solutions of transport problems. II. Convergence and applications of the discrete ordinate method. *J Soc Ind Appl Math* 1960;8:43–73.
- [27] Wendroff B. On the convergence of the discrete ordinate method. *J Soc Ind Appl Math* 1960;8:508–13.
- [28] Keller HB. On the pointwise convergence of the discrete ordinate method. *SIAM J Numer Anal* 1960;8:560–7.
- [29] Nelson Jr P. Convergence of the discrete-ordinates method for anisotropically scattering multiplying particles in a subcritical slab. *SIAM J Numer Anal* 1973;10:175–81.